Numerical evaluation of radiation and optical coupling occurring in optical coupler

Mansour Bacha[1,2,*] and Abderrahmane Belghoraf[1]

[1]*Electronics Department, University of Sciences and Technology of Oran Mohamed Boudiaf, Oran M'Naouer BP 1505, Algeria*

[2]*Centre of Satellites Development, Ibn Rochd USTO Oran BP 4065, Algeria*

**Corresponding author: bachamans@gmail.com*

Received August 26, 2016; accepted November 18, 2016; posted online February 1, 2017

We present in this work a new mathematical model to analyze and evaluate optical phenomena occurring in the nonuniform optical waveguide used in integrated optics as an optical coupler. By introducing some modifications to the intrinsic integral, we perfectly assess the radiation field present in the adjacent medium of the waveguide and, thus, follow the evolution of the optical coupling from the taper thin film to the substrate and cladding until there is a total energy transfer. The new model that is introduced can be used to evaluate electromagnetic field distribution in three mediums that constitute any nonuniform optical couplers presenting great or low wedge angles.

OCIS codes: 130.3120, 080.1510, 130.3130, 230.7370.

doi: 10.3788/COL201715.021301.

Optical waveguides constitute the basic elements of the integrated optical circuits. Their structure permit the confinement of light and the guiding of the energy flow of an electromagnetic wave in a direction parallel to their interfaces[1,2]. The optical propagation in the waveguide is maintained by the successive reflections on its interfaces. Among the multitude of waveguides that exist in the optical industry, we find nonuniform waveguides, which present a linear variation (decreasing or increasing) of the guiding film thickness. The waveguide that will be analyzed in this work is characterized by the decreasing of the guiding thin film; the optical rays of an incident beam undergo internal reflections on the interfaces of the waveguide until the waveguide cut-off, where the phenomenon of radiation becomes important, which allows light to be coupled from the nonuniform thin film to adjacent areas[2,3].

In this Letter, a new mathematical model based on the concept of intrinsic modes will be proposed with the aim to analyze and synthesize the propagation, radiation, and optical coupling that occur in a nonuniform thin film used as an optical coupler in integrated optics.

The mathematical model uses a spectral integral for assessing the behaviour of the optical waves within the nonuniform film of a greater refractive index, as well as outside the waveguide in the substrate and the cladding of lower refractive indexes[2,3].

The concept of intrinsic modes was first used in acoustic underwater applications[4,5], before its uses in integrated optics for the nonuniform structure[2,3,6–12]. To assess with a great precision the radiation and the optical coupling occurring in non uniform optical waveguide, some modifications will be introduced to the mathematical model already established for the intrinsic integral[2,3,6–12]. Intrinsic modes are solutions of Maxwell's equations, satisfying the boundary conditions at the interfaces between the different mediums[13]. The interest in the concept is because it allows for determining the electromagnetic field distribution in all mediums that constitute the waveguide, meaning the tapered thin film, the substrate, and the cladding.

In this Letter we will introduce some modifications to the mathematical model that is already established for the intrinsic integral[2,3,10–12].

Many classical analytical and numerical methods are used for the evaluation of the optical propagation in optical waveguides. We can cite, for example, the beam propagation method (BPM), the finite difference BPM (FDBPM), and the effective index method[2,14–19], but the method introduced in this Letter is global and universal and applicable for any nonuniform optical waveguide.

The basic structure of a tapered optical waveguide is shown in Fig. 1. It consists of a nonuniform thin film that serves as a waveguide of the refractive index (n_g), which is sandwiched by a substrate of the refractive index (n_s) and a cladding of the refractive index (n_c).

The refractive index values are defined as: $n_g > n_s > n_c$. The thickness W of the waveguide decreases linearly, and light is guided in the medium n_g by successive reflections on the waveguide boundaries.

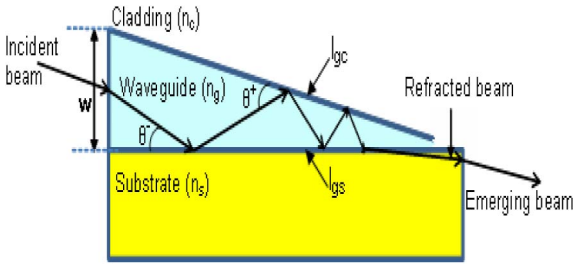

Fig. 1. Configuration of the optical coupler to analyze.

An incident ray in the nonuniform optical waveguide undergoes multiple reflections on the I_{gc} interface [tapered guide (n_g) and cladding (n_c)] and the I_{gs} interface [tapered guide (n_g) and a substrate (n_s)]. The angle of incidence increases gradually with the decreasing of the thickness of the waveguide 'W' (see Fig. 1).

Each pair of reflections on both interfaces increases the angle of incidence on I_{gc} (θ^+) and I_{gs} (θ^-) by adding twice the wedge angle 'a' formed by the two interfaces I_{gc} and I_{gs}, which means that m pairs of reflections on I_{gc} and I_{gs} will render the angles of incidence equal to $(\theta^{+-}) + 2\,ma$[2,3,10–12,20]. After several reflections on the interfaces I_{gc} and I_{gs}, the angle of incidence will be greater than the critical angle θ_c. There, we assist with a phenomena of radiation, and the energy will, thus, start to be coupled to the adjacent mediums n_c and n_s. This energy will increase with the arrival of the subsequent light rays to form a beam of light emerging in the adjacent mediums[3,20]. Because of the refraction of the energy of the nonuniform optical waveguide to the adjacent mediums (n_s) and (n_c), the waveguide is considered as an optical coupler in addition to its guiding property[2,20].

Some previous works using intrinsic modes[2,3,10–12] have considered the presence of total and perfect reflections at the I_{gc} interface, and they posed the phase of the Fresnel coefficient at the interface I_{gc} equal to π. In our study, we will treat the general case by using the exact phase of the Fresnel coefficient introduced at the I_{gc} interface, depending on the refracted index of each medium (n_g or n_c) to determine the modified intrinsic integral; this case was treated by Refs. [7,12,13], but they follow a different approach than those used by Refs. [6,8,9], and the mathematical expression found is different.

Using the complementary angles of that given in Refs. [2,20], the phases of the Fresnel coefficients introduced at I_{gc} and I_{gs} interfaces will be

$$\phi^{+-}(\theta^{+-}) = 2\,\arctan\left(\sqrt{\frac{n_g^2\cdot\cos^2(\theta^{+-}) - n_{c,s}^2}{n_g^2 - n_g^2\cdot\cos^2(\theta^{+-})}}\right). \tag{1}$$

From an incident ray positioned at X_0 to an observation point X, we will have four kinds of rays: those who go first towards I_{gc} and will have even or odd reflections at interfaces I_{gc} and I_{gs}, respectively, $W_e^+(X_0, X)$ and $W_o^+(X_0, X)$; and those who go first towards I_{gs} and will have even or odd reflections at interfaces I_{gc} and I_{gs}, respectively, $W_e^-(X_0, X)$ and $W_o^-(X_0, X)$[3,20].

The cumulative phases (Φ_{eo}^+) and (Φ_{eo}^-)[3] of waves directed first towards, respectively, the I_{gc} and I_{gs} interfaces, which undergo even or odd reflections, are given as[3,20]

$$\Phi_e^+(\theta_0,\theta_n) = \sum_{m=1}^{n}[\phi^+(\theta_m^+)] + \sum_{m=1}^{n}[\phi^-(\theta_m^-)], \tag{2}$$

$$\Phi_o^+(\theta_0,\theta_n) = \Phi_e^+(\theta_0,\theta_n) - \phi^-(\theta_n^-), \tag{3}$$

$$\Phi_e^-(\theta_0,\theta_n) = \sum_{m=1}^{n}[\phi^-(\theta_m^-)] + \sum_{m=1}^{n}[\phi^+(\theta_m^+)], \tag{4}$$

$$\Phi_o^-(\theta_0,\theta_n) = \Phi_e^-(\theta_0,\theta_n) - \phi^+(\theta_n^+), \tag{5}$$

where θ_0 is the first incident angle at interface I_{gs}, and θ_m is the incident angle at the mth reflection. n is the maximum number of reflections on the two interfaces.

The relation between θ_0 and θ_m after m reflections on interfaces I_{gc} and I_{gs} is[3,20]

$$\theta_m^{+-} = \theta_0^{+-} + 2\cdot a\cdot(m-1). \tag{6}$$

The integer m is defined as

$$m = 1 + \frac{\theta_m^{+-} - \theta_0^{+-}}{2\cdot a}. \tag{7}$$

By applying the Euler–Maclaurin formula[3,20,21] to Eqs. (3)–(5), we obtain discrete continuous sums:

$$\begin{aligned}\phi_e^+(\theta_0,\theta_n) = {}& \frac{1}{2}\phi^+(\theta_0^+) + \frac{1}{2}\phi^+(\theta_n^+) + \frac{1}{2\cdot a}\int_{\theta_0}^{\theta}\phi^+(\theta')\cdot\mathrm{d}\theta' \\ & + \frac{1}{2}\phi^-(\theta_0^-) + \frac{1}{2}\phi^-(\theta_n^-) \\ & + \frac{1}{2\cdot a}\int_{\theta_0}^{\theta}\phi^-(\theta')\cdot\mathrm{d}\theta' + E_e^+(\theta_n^+,\phi^+(\theta_n^+)) \\ & + E_e^+(\theta_n^-,\phi^-(\theta_n^-)),\end{aligned} \tag{8}$$

$$\begin{aligned}\phi_o^+(\theta_0,\theta_n) = {}& \frac{1}{2}\phi^+(\theta_0^+) + \frac{1}{2}\phi^+(\theta_n^+) + \frac{1}{2\cdot a}\int_{\theta_0}^{\theta}\phi^+(\theta')\cdot\mathrm{d}\theta' \\ & + \frac{1}{2}\phi^-(\theta_0^-) - \frac{1}{2}\phi^-(\theta_n^-) \\ & + \frac{1}{2\cdot a}\int_{\theta_0}^{\theta}\phi^-(\theta')\cdot\mathrm{d}\theta' + E_e^+(\theta_n^+,\phi^+(\theta_n^+)) \\ & + E_e^+(\theta_n^-,\phi^-(\theta_n^-)),\end{aligned} \tag{9}$$

$$\begin{aligned}\phi_e^-(\theta_0,\theta_n) = {}& \frac{1}{2}\phi^-(\theta_0^-) + \frac{1}{2}\phi^-(\theta_n^-) + \frac{1}{2\cdot a}\int_{\theta_0}^{\theta}\phi^-(\theta')\cdot\mathrm{d}\theta' \\ & + \frac{1}{2}\phi^+(\theta_0^+) + \frac{1}{2}\phi^+(\theta_n^+) \\ & + \frac{1}{2\cdot a}\int_{\theta_0}^{\theta}\phi^+(\theta')\cdot\mathrm{d}\theta' + E_e^-(\theta_n^-,\phi^-(\theta_n^-)) \\ & + E_e^-(\theta_n^+,\phi^+(\theta_n^+)),\end{aligned} \tag{10}$$

$$\begin{aligned}\phi_o^-(\theta_0,\theta_n) = {}& \frac{1}{2}\phi^-(\theta_0^-) + \frac{1}{2}\phi^-(\theta_n^-) + \frac{1}{2\cdot a}\int_{\theta_0}^{\theta}\phi^-(\theta')\cdot\mathrm{d}\theta' \\ & + \frac{1}{2}\phi^+(\theta_0^+) - \frac{1}{2}\phi^+(\theta_n^+) \\ & + \frac{1}{2\cdot a}\int_{\theta_0}^{\theta}\phi^+(\theta')\cdot\mathrm{d}\theta' + E_e^-(\theta_n^-,\phi^-(\theta_n^-)) \\ & + E_e^-(\theta_n^+,\phi^+(\theta_n^+)).\end{aligned} \tag{11}$$

In Eqs. (8)–(11), $E_e^+(\theta_n^+,\phi^+(\theta_n^+))$, $E_e^+(\theta_n^-,\phi^-(\theta_n^-))$, $E_e^-(\theta_n^-,\phi^-(\theta_n^-))$, and $E_e^-(\theta_n^+,\phi^+(\theta_n^+))$ are the errors introduced by the Euler–Maclaurin formula[3,11,21].

The use or not of the Euler–Maclaurin errors depends on the precision we want to have. But for the waveguides that have a large wedge angle 'a', it is recommended that these errors are calculated, which are expressed as[3,21]

$$E(\theta,\phi^{\pm}(\theta)) = 2\cdot\sum_{q=-\infty}^{+\infty}\left\{\frac{1}{2\cdot a}\int_{\theta_0}^{\theta}\phi^{\pm}(\theta')\cdot\cos\left[2\cdot\pi\cdot p\cdot\left(1+\frac{\theta'-\theta_0}{2a}\right)\right]\mathrm{d}\theta'\right\}. \quad (12)$$

The expressions of the four kinds of rays defined previously are[3,11]

$$W_e^+(X_0,X) = W_e^+(\theta_0,\theta) = \mathrm{Exp}\{j\cdot[\phi_e^+(\theta_0,\theta)+k\cdot R_e^+(\theta_0,\theta)]\}, \quad (13)$$

$$W_o^+(X_0,X) = W_o^+(\theta_0,\theta) = \mathrm{Exp}\{j\cdot[\phi_o^+(\theta_0,\theta)+k\cdot R_o^+(\theta_0,\theta)]\}, \quad (14)$$

$$W_e^-(X_0,X) = W_e^-(\theta_0,\theta) = \mathrm{Exp}\{j\cdot[\phi_e^-(\theta_0,\theta)+k\cdot R_e^-(\theta_0,\theta)]\}, \quad (15)$$

$$W_o^-(X_0,X) = W_o^-(\theta_0,\theta) = \mathrm{Exp}\{j\cdot[\phi_o^-(\theta_0,\theta)+k\cdot R_o^-(\theta_0,\theta)]\}. \quad (16)$$

where $R_e^+(\theta_0,\theta)$, $R_o^+(\theta_0,\theta)$, $R_e^-(\theta_0,\theta)$, and $R_o^-(\theta_0,\theta)$ are the geometrical lengths defined as[3,10,20]

$$R_p^+(\theta_0,\theta_m) = r_0\cdot\cos(\theta_0-a-x_0)-r\cdot\cos(\theta+a-x), \quad (17)$$

$$R_i^+(\theta_0,\theta_m) = r_0\cdot\cos(\theta_0-a-x_0)-r\cdot\cos(\theta-a+x), \quad (18)$$

$$R_p^-(\theta_0,\theta_m) = r_0\cdot\cos(\theta_0-a+x_0)-r\cdot\cos(\theta-a+x), \quad (19)$$

$$R_i^-(\theta_0,\theta_m) = r_0\cdot\cos(\theta_0-a+x_0)-r\cdot\cos(\theta+a-x). \quad (20)$$

We obtained the modified intrinsic integral as a spectrum of all incident waves inside the optical waveguide after using the Poisson transformation[3,10,20]:

$$W(\theta_0,\theta) = \frac{1}{2a}\int_c\sum_{q=-\infty}^{+\infty}\{[W_e^+(\theta_0,\theta)+W_o^+(\theta_0,\theta)+W_e^-(\theta_0,\theta)+W_o^-(\theta_0,\theta)]\cdot\mathrm{Exp}(-j\cdot2\pi\cdot q\cdot m)\}\mathrm{d}\theta. \quad (21)$$

In Eq. (17), the term 'q' represents the mode number.

To simplify the evaluation, we will normalize the new model of the modified intrinsic integral. The normalized model will be applied to evaluate the propagation inside any tapered waveguide independently of the position of the source, which is considered as source-free[2,3,5,8–11,20]. This can be explained by the fact that by considering it source-free, its constant parameters will have a constant influence in the phase of the modified intrinsic integral.

Because of the interdependence of the four waves that are defined, we can evaluate the modified intrinsic integral in two manners, by waves going first towards the upper interface or waves first going down, as following[3,20].

For the first case, we will have at any observation point in the waveguide (n_g) as

$$W^+(X,\theta) = \frac{1}{2a}\int_c\{[W_e^+(X,\theta)+W_o^+(X,\theta)]\cdot\mathrm{Exp}(-j\cdot2\pi\cdot q\cdot m)\}\mathrm{d}\theta, \quad (22)$$

$$W^-(X,\theta) = \frac{1}{2a}\int_c\{[W_e^-(X,\theta)+W_o^-(X,\theta)]\cdot\mathrm{Exp}(-j\cdot2\pi\cdot q\cdot m)\}\mathrm{d}\theta. \quad (23)$$

The two equations give us the variation of the field inside the nonuniform waveguide. The field variations in the substrate and the cladding are given after adding the Fresnel transmission coefficient (right side of the integral) at each interface[3,5–7,20] as

$$W_s(X,\theta) = \frac{1}{2a}\int_c\sum_{q=-\infty}^{+\infty}\{[1+\mathrm{Exp}(j\cdot\phi^-)]\cdot W_o^+(X,\theta)\,\mathrm{Exp}(-j\cdot2\pi\cdot q\cdot m)\}\mathrm{d}\theta, \quad (24)$$

$$W_s(X,\theta) = \frac{1}{2a}\int_c\sum_{q=-\infty}^{+\infty}\{[1+\mathrm{Exp}(j\cdot\phi^+)]\cdot W_o^-(X,\theta)\,\mathrm{Exp}(-j\cdot2\pi\cdot q\cdot m)\}\mathrm{d}\theta. \quad (25)$$

The numerical evaluation of the new mathematical model given in Eqs. (18)–(20) is very difficult, because we are in the presence of integrals using complex functions. Various methods can be used to approximately assess the spectral integral $W(X,\theta)$: we can name the steepest descent path (SDP), the fast Fourier transform (FFT), and the numerical method consisting of integration directly along the real axis of the incident angles θ in the interval $(0<\theta<\pi/2)$[3,4,10,11,13,20,22]. In our case, we will approximately evaluate the modified intrinsic integral by integration directly on the real axis because this numerical method is less difficult and more rapid than the others, and it permits for the computation of the electromagnetic field both in the propagation region and the leaky wave region[2,3,10,20,23]. One has to note that in this work, we have used the transverse electric (TE) mode, and the same approach can be used in the transverse magnetic (TM) mode.

Figures 2 and 3 represent the electromagnetic distribution field in three regions of a symmetric polymer waveguide constituted by a polymer tapered thin film of the refractive index $n_g = 1.77$, which is surrounded by a substrate and a cladding silica (SiO_2) of the refractive index

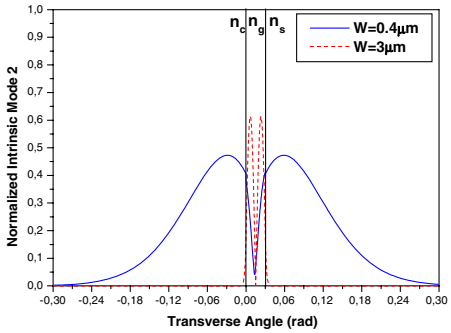

Fig. 2. Second intrinsic normalized mode ($q = 2$) of a symmetric polymer optical waveguide for the wedge angle $a = 0.03$ rad. The dashed graph represents the normalized intrinsic field at a thickness of $W = 3$ μm, and the solid line represents the intrinsic field at thickness $W = 0.4$, which is lower than the cut-off thickness.

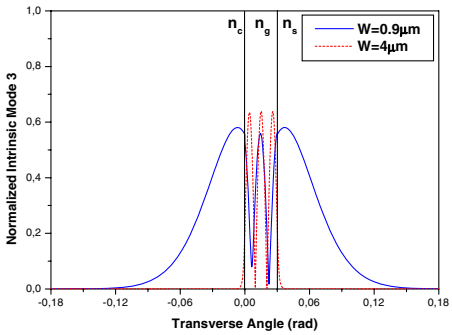

Fig. 3. Third intrinsic normalized mode ($q = 3$) of a symmetric polymer optical waveguide for the wedge angle $a = 0.03$ rad. The dashed graph represents the normalized intrinsic field at a thickness of $W = 4$ μm, and the solid line represents the field at a thickness of $W = 0.9$, which is lower than the cut-off thickness.

$n_s = n_c = 1.45$ at the wavelength $\lambda = 1$ μm[22]. In Figs. 2 and 3, the intrinsic field is normalized to a maximum value of each mode (second and third mode), and the field distribution is as follows: $x < 0$ rad in the substrate (n_s), $0 < x < 0.03$ rad in the tapered thin film (n_g), and $x > 0.03$ rad in the cladding (n_c).

The dashed graph in Fig. 2 represents the intrinsic field distribution before the waveguide cut-off at the waveguide thickness of $W = 3$ μm, and the solid line graph represents the field distribution after the waveguide cut-off at the waveguide thickness of $W = 0.4$ μm.

We can note that in Fig. 2 there is symmetry in the distribution of the intrinsic field in the substrate and the cladding. Before the waveguide cut-off, the field is concentrated in the guide n_g, but after the cut-off, we assist in an optical coupling of the field by radiation in the adjacent mediums (n_s and n_c), which is constituted of substrate and cladding in a symmetric way. The same remark can be made for the third mode represented by Fig. 3.

Figures 4 and 5 show exactly how the optical coupling occurs from the tapered waveguide to the adjacent mediums by the radiation phenomena for two symmetric waveguides. The first waveguide is the AlAsGa/AsGa/AlAsGa

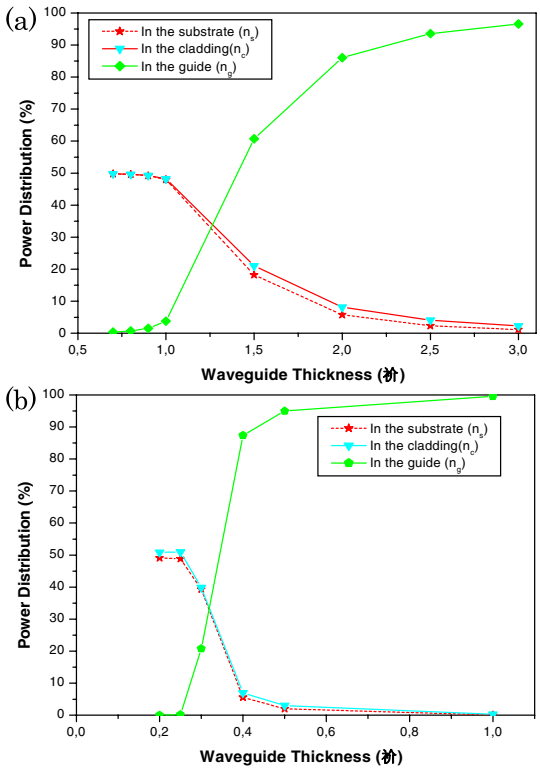

Fig. 4. Power distribution in the three regions of a symmetric tapered waveguide for the mode $q = 3$ and a wedge angle $a = 1°$ for (a) the waveguide AlAsGa/AsGa/AlAsGa and (b) the waveguide $SiO_2/Si/SiO_2$.

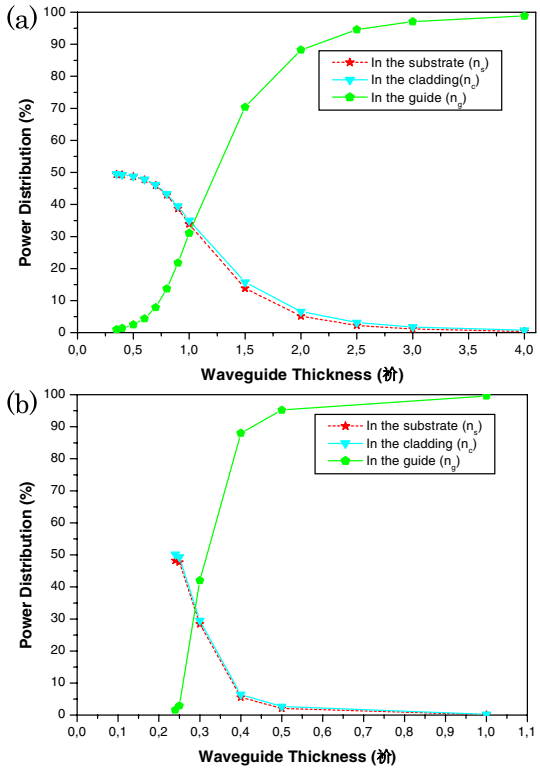

Fig. 5. Power distribution in the three regions of a symmetric tapered waveguide for the mode $q = 3$ and a wedge angle $a = 5°$ for (a) the waveguide AlAsGa/AsGa/AlAsGa and (b) the waveguide $SiO_2/Si/SiO_2$.

with $n_{g(\mathrm{AsGa})} = 3.44$, $n_{c,s(\mathrm{AlAsGa})} = 3.36$ at $\lambda = 1.55$ μm[18], and the second waveguide is $SiO_2/Si/SiO_2$ with $n_{g(\mathrm{Si})} = 3.5$ and $n_{c,s(SiO_2)} = 1.447$ at $\lambda = 1.3$ μm[24,25].

Figure 4 represents the power distribution of the third mode in three regions of the waveguide with the wedge angle $a = 1° = 0.0174$ rad.

Figure 5 illustrates the power distribution of the third mode with the wedge angle $a = 5° = 0.087$ rad.

In Figs. 4 and 5, we assist with a gradual power transfer from the tapered waveguide to the adjacent mediums. But at thicknesses lower than the cut-off thickness of each mode, we see a fast power transfer until a total optical coupling.

We remark in Fig. 5 that for a larger wedge angle (5°), the total power transfer occurs at lower waveguide thicknesses, compared to a smaller angle (1°), but in all cases, there is power conservation in the three waveguide regions.

The results shown in Figs. 4 and 5 demonstrate the interest and the power of the method introduced in this Letter, and by applying it, one can efficiently follow the behavior of the optical waves both inside and outside of the optical waveguide.

In conclusion, the new model introduced in this Letter permits for the prediction of the behavior of light waves as they propagate throughout a nonuniform structure, and thus allows for determining the electromagnetic field distribution in all media constituting the nonuniform optical waveguide for different refractive indexes and different wedge angles formed by the waveguide interfaces.

In addition to modelling the propagation and the radiation of the electromagnetic field, the computation of the modified intrinsic integral also allows for a systematic evaluation of the optical coupling phenomena occurring in an optical coupler. The new intrinsic model can be used to modulate all types of nonuniform optical waveguides that are constituted by any optical materials and any wedge angles.

This work was co-supported by the University of Sciences and Technology of Oran Mohamed Boudiaf (USTOMB) and the Centre of Satellites Development (CDS), Oran, Algeria.

References

1. A. Boudrioua, *Photonic Waveguides Theory and Applications* (ISTE, 2009).
2. M. Bacha and A. Belghoraf, Chin. Opt. Let. **12**, 070801 (2014).
3. A. Belghoraf, "Analysis of the Tapered Waveguide," Ph.D. thesis (Université de Nottingham, 1984).
4. A. Kamel and L. B. Fielsen, J. Acoust. Soc. Am. **73**, 1120 (1983).
5. J. Arnold and A. Ansbro, Journal de Physique Colloques **51**, C2-953 (1990).
6. J. M. Arnold, A. Belghoraf, and A. Dendane, IEE Proc. **132**, 314 (1985).
7. A. Dendane and J. M. Arnold, IEEE J. Quantum Electron. **QE-22**, 1551 (1986).
8. M. Cada, F. Xiang, and L. B. Felson, IEEE J. Quantum Electron. **24**, 758 (1988).
9. M. Cada, F. Xiang, and L. B. Felson, IEEE J. Quantum Electron. **25**, 933 (1989).
10. A. Belghoraf, AMSE Periodicals: Modell., Meas. Control. A **45**, 21 (1992).
11. A. Belghoraf, AMSE J. Mod. Meas. Control, General Phys. **74**, 51 (2001).
12. M. Bacha and A. Belghoraf, Int. Rev. Mod. Simul. **6**, 1624 (2013).
13. J. M. Arnold and A. Dendane, IEE Proc. **136**, 250 (1989).
14. V. Prajzler, H. Tuma, J. Spirkova, and V. Jerabek, Radioengineering **22**, 233 (2013).
15. K. Kawano and T. Kitoh, *Introduction to Optical Waveguide Analysis: Solving Maxwell's Equations and the Schrödinger Equation* (Wiley, 2001).
16. G. L. Yip, Integr. Opt. Circuits SPIE **1583**, 240 (1991).
17. Y. T. Han, J. U. Shin, D. J. Kim, S.-H. Park, Y.-J. Park, and H.-K. Sung, ETRI J. **25**, 535 (2003).
18. M. M. Ismail and M. N. Shah Zainuddin, Appl. Mech. Mater. **52–54**, 2133 (2011).
19. R. Tao, X. Wang, H. Xiao, P. Zhou, and L. Si, Photon. Res. **1**, 186 (2013).
20. M. Bacha and A. Belghoraf, Prog. Electromagn. Res. M **51**, 175 (2016).
21. F. W. J. Olver, *Asymptotic and Special Functions* (Academic, 1974).
22. J.-M. Liu, *Photonic Devices* (Cambridge University, 2005).
23. A. Belghoraf and M. Bacha, Int. Res. J. Eng. Technol. (IRJET) **3**, 3049 (2016).
24. http://refractiveindex.info/?shelf=main&book=Si&page=Li-293K.
25. http://refractiveindex.info/?shelf=main&book=SiO2&page=Malitson.